Journal of Brilliant Engineering 1 (2027) 41158

Brilliant Engineering

journal home: www.acapublishing.com/journals/4/ben

Research Article

Design of a Thin-Profile FR-4 Based Multi-Band Metasurface Absorber in S, C, X, and Ku Bands

Merve Kurt*,[1]

[1]Ataturk University, Department of Electrical and Electronics Engineering, Erzurum, Türkiye

Keywords

Metasurface absorber,
Microwave absorber,
Multi-band absorption,
Polarization-independent design,
Wide-angle incidence.

Abstract

This study numerically presents the design of a multi-band metasurface-based microwave absorber designed to operate in the S, C, X, and Ku bands. The proposed structure exhibits simulated peak absorption values above 95% at resonance frequencies of 2.9 GHz, 6.3 GHz, 11.7 GHz, and 17.5 GHz, with narrowband fractional bandwidths of 0.64–1.14%. Polarization sensitivity was evaluated under normal incidence, while angular stability was assessed for Transverse Electric (TE) and Transverse Magnetic (TM) modes under oblique incidence. In addition, the structure was analyzed at oblique incidence angles of 15°, 30°, 45°, 60°, and 75° for TE and TM modes, showing that high absorption performance is generally maintained up to 60° incidence. To further interpret the absorption mechanism, effective permittivity and effective permeability were retrieved at the resonance frequencies; because the design is metal-backed, these parameters are treated as qualitative indicators of the electric and magnetic resonances rather than bulk constitutive parameters. Normalized impedance analysis confirms good matching with free space, with the real part approaching unity and the imaginary part approaching zero at all four resonances. In addition, electric field, magnetic field, and surface current distributions were analyzed at each resonance frequency, revealing anti-parallel current loops between the patterned resonator and the ground plane that confirm the magnetic-resonance mechanism underlying the absorption response. An equivalent circuit model (ECM) was additionally constructed in ADS to verify the reliability of the simulation results, yielding a reflection coefficient (S11) response consistent with the CST Microwave Studio results.

1. Introduction

With the development of electromagnetic technologies, the control of electromagnetic waves in microwave and radar frequency bands has become an important research area. Radar Cross Section (RCS) reduction plays a significant role in stealth technologies, as it helps make military vehicles less detectable by radar systems [1]. In addition, microwave absorber structures are widely used in civilian applications such as reducing electromagnetic interference (EMI) and ensuring electromagnetic compatibility (EMC), improving the performance of wireless communication systems, and protecting electronic devices [2]. While these represent important application-level motivations for absorber research, it should be noted that realizing these application-level benefits (e.g., RCS reduction, EMI/EMC mitigation) in a specific absorber design requires dedicated application-specific simulations or measurements beyond the unit-cell characterization presented in this study.

For these purposes, metamaterials — artificially engineered structures with electromagnetic properties not found in natural materials — have been widely investigated. The field was pioneered by Veselago, who predicted that a negative refractive index can be achieved when permittivity (ε) and permeability (μ) are simultaneously negative [3]; Pendry later realized structures exhibiting negative permittivity and permeability [4,5], and Smith and colleagues demonstrated the first left-handed metamaterial by combining these properties [6]. Metamaterials have since enabled diverse functionalities, including frequency filtering [7], polarization control [8], and electromagnetic energy absorption, in which incident waves are dissipated as heat rather than reflected or transmitted [9]. These properties have found application in antennas [10], sensors [11], optical systems [12], cloaking [13], biomedical technologies [14], and radar systems [15], with metamaterial-based microwave absorbers reported across both GHz [16] and THz [17] frequency ranges. Absorber performance is typically evaluated in terms of substrate material, number of operating bands, polarization independence, oblique-incidence behavior, and structural thickness, and broadband [18] or multiband [19] operation has been pursued using thin films [20], lumped RLC elements [21], multilayer structures [22], and single-layer designs [20]. Considerable recent effort has focused on metamaterial absorbers that combine high absorption, wide-angle operation, and polarization insensitivity.

The performance of a metasurface absorber (MSA) is influenced by several parameters such as resonator geometry, dielectric material properties, layer thickness, and material losses. In this study, considering these design criteria, a single-layer metasurface absorber (MSA) structure is proposed, consisting of a continuous metallic ground plane on the backside that blocks electromagnetic transmission and a resonator on the top surface that reduces reflection and enables absorption. The electromagnetic performance of the proposed structure is simulated and analyzed using CST Microwave Studio. Although numerous multi-band, polarization-insensitive FR-4-based metasurface absorbers have been reported in the literature, simultaneously achieving S-, C-, X-, and Ku-band absorption within a single-layer structure with a sub-0.01λ_0 electrical thickness — while maintaining polarization insensitivity over the full 0°–90° range and angular stability up to 60° — remains a significant design challenge. The novelty of this study lies in the specific square-frame/cross-shaped resonator combination that simultaneously satisfies these four performance criteria within a single 1 mm FR-4 layer.

*Corresponding Author: merve.kurt025@gmail.com
Received 17 Jun 2026; Revised 18 Aug 2026; Accepted 19 Aug 2026 https://doi.org/10.36937/ben.2027.41158

To explicitly state the novelty of the proposed design: the new design principle is the co-location, within a single 1 mm FR-4 layer, of an outer square-frame resonator and an inner cross-shaped resonator that independently control the lower/mid-frequency (2.9 and 11.7 GHz) and higher-frequency (6.3 and 17.5 GHz) resonances through longer and shorter current paths, respectively, enabling four-band operation from a single patterned layer rather than a multilayer or multi-cell stack; relative to the works compared in Table 4, the proposed design does not achieve the highest peak absorption (some reported designs exceed 99%) or the widest angular range (up to 80° in one case), but it achieves the smallest normalized substrate thickness (0.009λ0) among all compared designs while simultaneously covering four bands and maintaining polarization insensitivity over the full 0°–90° range; the novelty therefore lies primarily in the resonator geometry and the resulting electrical thickness — i.e., in achieving four-band coverage, sub-0.01λ0 thickness, and full-range polarization insensitivity simultaneously — rather than in any single record-breaking metric; no fundamentally new absorption physics is introduced: the design relies on the well-established metal-backed metasurface mechanism in which anti-parallel currents between the patterned resonator and the ground plane produce magnetic (LC-type) resonances, as discussed in Section 3; and no new optimization algorithm is proposed: the final geometry was obtained through parametric sweeps of the resonator dimensions, as presented in Figure 9, rather than through a genetic algorithm, particle swarm, or gradient-based optimizer.

2. Material and Method

In the designed MSA, an FR-4 substrate with a thickness of 1 mm was employed as the dielectric material. The FR-4 substrate has a relative permittivity of 4.3 and a loss tangent of 0.025, corresponding to standard manufacturer-datasheet values for this material and commonly adopted as constant, frequency-independent parameters in the microwave-absorber literature over the 1–20 GHz range; although FR-4 permittivity and loss tangent can vary slightly with frequency and between manufacturers, this variation is small relative to the resonance bandwidths of the proposed absorber and is not expected to alter the reported resonance frequencies or peak-absorption trends significantly. A dedicated dielectric-dispersion and manufacturer-tolerance sensitivity analysis is beyond the numerical scope of the present study, which is restricted to the nominal-parameter unit-cell response. The reported results correspond to the nominal FR-4 and copper parameters listed above; a fabrication-tolerance sensitivity analysis covering copper line-width variation (±0.05 mm), substrate-thickness variation (±0.05 mm), FR-4 relative-permittivity variation (4.1–4.5), loss-tangent variation (0.015–0.035), and copper-conductivity variation is outside this scope. To enhance the electromagnetic absorption performance and suppress transmission, the bottom surface of the structure was fully covered with a copper layer having an electrical conductivity of 5.8×10^7 S/m and a thickness of 0.035 mm. The resonator located on the top surface was also fabricated using copper with the same electrical conductivity. The simulations were performed using the frequency-domain solver of CST Microwave Studio with the General-Purpose broadband sweep method and a tetrahedral mesh. Adaptive tetrahedral mesh refinement was employed with a minimum of 3 and a maximum of 8 passes; convergence was checked against two criteria — an absolute S-parameter deviation threshold of 0.02 and an absolute Floquet port-mode (kz/k0) deviation threshold of 0.005 between successive passes — both of which were satisfied prior to the final solution. The excitation was defined using Floquet port boundary conditions (All + Floquet mode) over the 1–20 GHz frequency range. Copper layers were modeled as a lossy metal with an electrical conductivity of $\sigma = 5.8 \times 10^7$ S/m; surface roughness was not included in the model, and an ideally smooth conductor surface was assumed.

The unit-cell geometry of the proposed MSA was defined by a periodicity of p = 11 mm, an outer frame length of d = 10.8 mm, a conductive strip width of m = 0.8 mm, and inner structural dimensions of l = 2.68 mm, n = 1.6 mm, k = 1.3 mm, s = 2.8 mm, b = 3.1 mm, and c = 3.6 mm. The dielectric layer thickness was selected as h = 1 mm. To determine these geometrical parameters, extensive parametric analyses were conducted, and the dimensions providing the optimum absorption performance were obtained through an optimization process. The parametric sweep results, showing the individual effect of each geometrical parameter (p, k, s, c, and h) on the S_{11} response, are presented in Figure 9; the final dimensions were selected, through iterative manual sweeps, as those that jointly maximized the peak absorption at the four target resonances while preserving adequate frequency separation between bands.

The proposed geometry was formed by incorporating square- and cross-shaped resonator elements inside the outer square frame with a side length of d. This geometrical configuration promotes the excitation of multiple resonant modes at different frequencies, enabling efficient absorption of incident electromagnetic waves. Furthermore, selecting the dielectric layer thickness as 1 mm allowed the realization of a low-profile structure while maintaining the desired resonance characteristics. The scaled top and side views of the proposed MSA are presented in Figure 1.

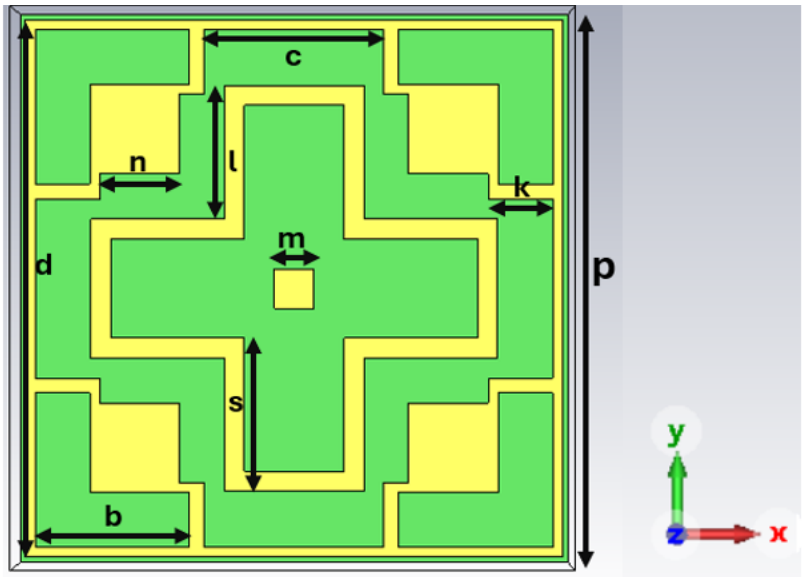

Figure 1. Geometrical configuration and dimensional parameters of the proposed MSA unit cell

At microwave frequencies, scattering parameters (S-parameters) are widely used to characterize the electromagnetic behavior of a structure. These parameters allow the determination of how much of the incident electromagnetic wave is reflected and transmitted by the structure. The absorption performance of the MSA can be calculated using the reflection (S_{11}) and transmission (S_{21}) coefficients, as given in Equation (1) [23].

$$A(\omega) = 1 - |S_{11}(w)|^2 - |S_{21}(w)|^2 = 1 - R(\omega) - T(\omega) \quad (1)$$

Here, $A(\omega)$ denotes the frequency-dependent absorption, $R(\omega) = |S_{11}(w)|^2$ the power reflection coefficient (reflectance), and $T(\omega) = |S_{21}(w)|^2$ the power transmission coefficient (transmittance). Because the proposed structure employs a metal–dielectric–metal configuration with a fully conductive copper ground plane, electromagnetic wave transmission through the structure is effectively prevented. Therefore, T(ω) ≈ 0, and the absorption expression simplifies to: $A(\omega) \approx 1 - |S_{11}(w)|^2 \approx 1 - R(\omega)$.

The assumption that S21 ≈ 0 is further supported mathematically by considering the skin depth of copper. At the lowest operating frequency of 2.9 GHz, the skin depth of copper (conductivity σ = 5.8 × 10^7 S/m) is $\delta = \frac{1}{\sqrt{\pi * f * \mu_0 * \sigma}} \approx 1.23$ μm , where δ is the skin depth, f is the operating frequency, μ_0 is the permeability of free space, and σ is the electrical conductivity of copper, which is more than 28 times smaller than the 35 μm (0.035 mm) copper thickness used for both the ground plane and the top resonator. Because the metal thickness is thus much greater than the skin depth even at the lowest frequency of interest, the copper layers behave as effectively opaque conductors across the entire 1–20 GHz simulation band, mathematically confirming this assumption.

To characterize electromagnetic behavior, it is necessary to determine structural parameters such as effective permittivity (ε_{ff}) and effective permeability (μ_{eff}). These parameters are fundamental quantities that directly represent the material's response to electromagnetic waves as well as its inherent loss mechanisms. In this approach, the electromagnetic characteristics of the metamaterial structure can be retrieved through an inverse retrieval method based on S-parameters [24].

For the proposed metasurface absorber (MSA), the effective structural parameters (ε_{ff}, μ_{eff}) are expressed as a function of the S-parameters as given in Equations (2) and (3).

$$\varepsilon_r = \frac{2}{jwd}\frac{1-(S_{21}+S_{11})}{1+(S_{21}+S_{11})} \quad (2)$$

$$\mu_r = \frac{2}{jwd}\frac{1-(S_{21}-S_{11})}{1+(S_{21}-S_{11})} \quad (3)$$

Here, k_0 denotes the free-space wave number, and $d$represents the thickness of the structure. The effective refractive index $n_{\text{eff}} = \sqrt{\mu_{\text{eff}}\,\varepsilon_{\text{eff}}}$ is a fundamental parameter that determines the propagation characteristics of electromagnetic waves within the structure and has a direct influence on both the amplitude and phase behavior of the wave.

A key parameter in the design of metasurface absorbers (MSAs) is the normalized impedance. When an electromagnetic wave transitions from free space into a metasurface structure, impedance mismatch leads to reflection. Therefore, for efficient absorption, the impedance of the structure should be close to the impedance of free space.

The normalized impedance is defined using the S-parameters as given in Equation (4).

$$Z = \sqrt{\frac{\mu_{eff}}{\varepsilon_{eff}}} = \sqrt{\frac{(1+S_{11})^2-(S_{21})^2}{(1-S_{11})^2-(S_{21})^2}} \quad (4)$$

Here, Z denotes the normalized impedance value of the MSA.

The retrieval procedure described by Equations (2)–(4) is based on the conventional two-port transmission–reflection inversion method, which is applicable when both the reflection coefficient (S_{11}) and the transmission coefficient (S_{21}) provide independent electromagnetic information. For the proposed metal-backed metasurface absorber, the continuous metallic ground plane suppresses electromagnetic transmission, resulting in $S_{21} \approx 0$. Under this condition, the retrieval of the effective permittivity, effective permeability, and refractive index becomes numerically ill-conditioned because these parameters depend on both reflection and transmission coefficients. Consequently, these retrieved quantities are used only as qualitative indicators of the electric and magnetic resonances rather than as rigorous bulk constitutive parameters of the metasurface. In contrast, the normalized wave impedance can be obtained directly from the one-port reflection coefficient, Z = $(1+S_{11})/(1-S_{11})$, which coincides with the $S_{21} \rightarrow 0$ limit of Equation (4). During the refractive-index retrieval, the appropriate branch of the inverse cosine function is determined by satisfying the passivity condition, $\mathrm{Im}(n) \geq 0$, ensuring physically meaningful solutions for a passive and causal medium. The discontinuities observed in the retrieved parameters near the resonance frequencies arise from the branch-selection (phase-unwrapping) procedure, combined with high numerical sensitivity to the near-zero S_{21} values. Therefore, these discontinuities should be regarded as numerical artifacts of the retrieval process rather than as physical characteristics of the proposed metasurface. The homogenized bulk interpretation remains a reasonable approximation in this context because the unit-cell periodicity (p = 11 mm) remains smaller than the free-space wavelength at all four resonance frequencies (p/λ_0 ≈ 0.11–0.64 over 2.9–17.5 GHz), which reasonably supports an effective-medium interpretation at the lower bands (S, C, and X); however, at 17.5 GHz (Ku-band) the ratio approaches p/λ_0 ≈ 0.64, indicating that the homogenization assumption becomes weaker at the highest frequency and the retrieved parameters there should be interpreted with additional caution, consistent with their treatment as qualitative rather than intrinsic material properties throughout this study.

3. Results and Discussion

In this study, the electromagnetic performance of the proposed MSA is numerically investigated using CST Microwave Studio. In the simulations, the structure is assumed to be periodically repeated, and a single unit cell model is employed with Floquet port boundary conditions. The analyses are carried out in the frequency domain.

A plane electromagnetic wave is used for excitation. The electric field (E) is oriented along the y-direction, the magnetic field (H) along the x-direction, and the wave propagation direction (k) along the z-direction. The study is conducted in the 1–20 GHz frequency range.

This periodic unit-cell approach with Floquet boundary conditions provides an idealized representation of an infinite array under plane-wave illumination. It should be noted that this model does not account for finite-array edge effects, fabrication tolerances, mounting conditions, or finite-beam illumination encountered in practical deployment; therefore, the presented results should be interpreted as the theoretical performance of the unit cell rather than a direct prediction of finite-panel behavior. Quantifying edge-truncation and mutual-coupling effects — for example, through a finite-array simulation of a 10×10, 15×15, or 20×20 unit-cell panel under plane-wave illumination — lies outside the scope of the present unit-cell characterization. The obtained results are presented in Figure 2. According to the results, the proposed MSA exhibits high absorption of 99.4%, 97.9%, 98.2%, and 95.1% at 2.9 GHz, 6.3 GHz, 11.7 GHz, and 17.5 GHz, respectively. These resonance frequencies correspond to the S, C, X, and Ku bands, respectively.

To quantitatively evaluate the narrowband characteristics of the absorption peaks, the −10 dB reflection bandwidth, the 80% and 90% absorption bandwidths, the fractional bandwidth (FBW = BW/f × 100), and the quality factor (Q = fc/BW) were calculated for each resonance frequency and are summarized in Table 1. The results show that the narrowest bandwidth is obtained at 2.9 GHz with a bandwidth of 19 MHz (FBW = 0.64%), whereas the widest bandwidth is observed at 11.72 GHz with a bandwidth of 133 MHz (FBW = 1.14%). The corresponding quality factor values range from 88 to 157, confirming that the proposed design exhibits high-Q narrowband resonances rather than broadband absorption. In terms of electrical size, the substrate thickness h = 1 mm corresponds to an electrical thickness h/λ_0 of approximately 0.0097 at 2.9 GHz, 0.021 at 6.3 GHz, 0.039 at 11.7 GHz, and 0.058 at 17.5 GHz, while the unit-cell periodicity p = 11 mm corresponds to an electrical unit-cell size p/λ_0 of approximately 0.106, 0.231, 0.429, and 0.642 at these four frequencies, respectively. These values confirm that the absorber remains electrically thin and the unit cell remains sub-wavelength across the S-, C-, and X-bands, while the periodicity approaches roughly two-thirds of a free-space wavelength at the highest (Ku-band) resonance, which is also why the effective-parameter homogenization is treated with additional caution at 17.5 GHz, as noted above.

Table 1. Bandwidth and quality-factor characteristics of the four absorption resonances

Resonance	f (GHz)	Peak Performance (%)	-10dB BW (MHz)	FBW (%)	Q-Factory	Peak >80% BW (MHz)	Peak >90% BW (MHz)
1	2.9	99.4	19	0.64	156.6	38	19
2	6.3	97.9	57	0.90	111.2	95	57
3	11.7	98.2	133	1.14	88.1	228	133
4	17.5	95.1	114	0.65	154.1	209	114

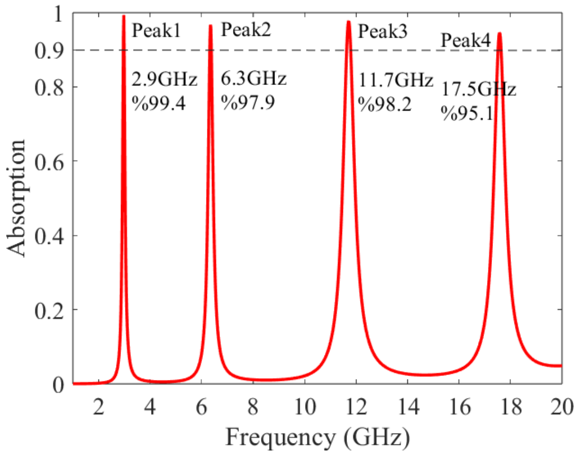

Figure 2. CST-simulated absorption performance of the proposed MSA unit cell

In Figure 3(a–b), the absorption results for TE and TM modes at different incidence angles between 0° and 75° are presented with 15° increments. The results demonstrate that the proposed metasurface structure maintains over 80% absorption at incidence angles up to 60°, as quantitatively confirmed for all resonances and modes in Table 2.

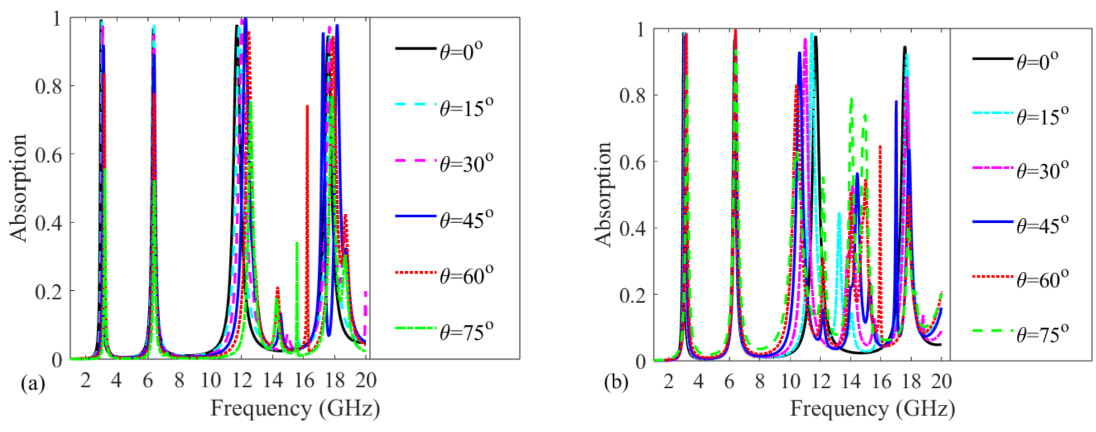

Figure 3. Absorption performance of the proposed MSA at different incidence angles (0°–75°) with 15° increments: (a) TE mode, (b) TM mode

Figure 4(a–b) presents the absorption performance of the proposed MSA under different polarization angles for TE and TM modes. The results indicate that the absorption performance remains nearly unchanged despite variations in the polarization angle. As quantified in Table 3, the absorption magnitude at each resonance varies by no more than approximately 0.4 percentage points across all tested polarization angles (0°, 30°, 60°, and 90°) for both TE and TM modes. This behavior demonstrates the polarization-insensitive characteristic of the proposed structure.

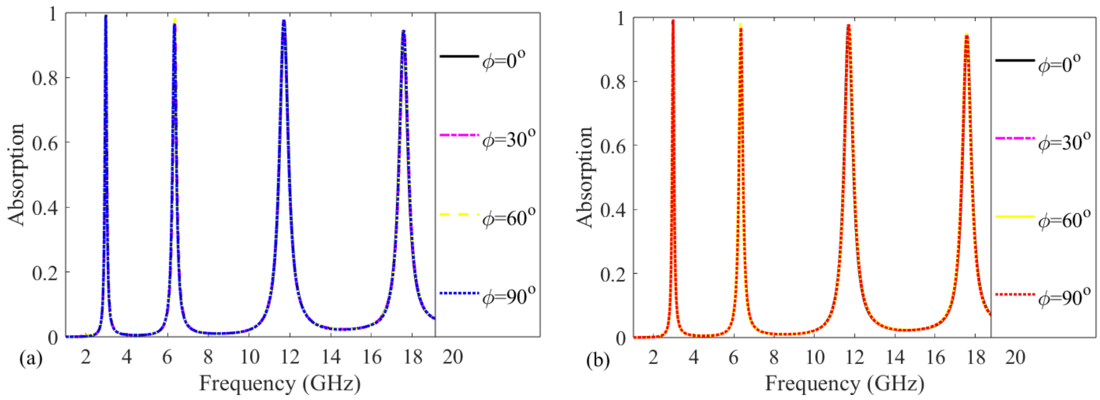

Figure 4. Absorption performance of the proposed MSA under different polarization angles for TE and TM modes: (a) TE mode, (b) TM mode

The numerical performance results of the proposed absorber under different oblique incidence angles and polarization angles are presented in Tables 2 and 3, respectively, including the corresponding resonance frequencies and absorption rates.

Table 2. Performance results of the proposed absorber under different oblique incidence angles for TE and TM polarizations

Incidence Angles	Mode	Absorption Performance f_1	Absorption Performance f_2	Absorption Performance f_3	Absorption Performance f_4
0°	TE	2.9 GHz- % 99.4	6.3 GHz- 97.9 %	11.7 GHz -98.2%	17.6 GHz -95.1%
15°	TE	2.9 GHz- %98.8	6.3 GHz- %97	11.8 GHz- %98	17.6 GHz- %95
30°	TE	3.1 GHz- %97	6.4 GHz- %94	12 GHz- %98	17.6 GHz- %95
45°	TE	3.1 GHz- %92	6.4 GHz- %90	12.3 GHz- %91	17.2 GHz- %94
60°	TE	3.1 GHz- %84	6.4 GHz- %80	12.5 GHz- %91	17.7 GHz- %93
75°	TE	3.2 GHz- %50	6.3 GHz- %53	12.6 GHz- %74	17.8 GHz- %74
0°	TM	2.9 GHz- 99.4%	6.3 GHz- 97.9 %	11.7 GHz -98.2%	17.6 GHz -95.1%
15°	TM	2.9 GHz- %99	6.3 GHz- %97	11.4 GHz- %98	17.7 GHz- %93
30°	TM	3 GHz- %97	6.3 GHz- %97	11.4 GHz- %96	17.7 GHz- %90
45°	TM	3.1 GHz- %97.2	6.3 GHz- %96	11.1 GHz- %92	17 GHz- %90
60°	TM	3.1 GHz- %97.6	6.4 GHz- %97	10.8 GHz- %80	17.8 GHz- %79.6
75°	TM	3.2 GHz- %84	6.4 GHz- %93	12.2 GHz- %50	17.8 GHz- %63

To further quantify the angular stability, the frequency shift was evaluated as $\Delta f(\%) = |f_\theta - f_0|/f_0 \times 100$, where f_0 and f_θ denote the resonance frequency at normal incidence and at oblique incidence angle θ, respectively. Based on Table 2, at 60° incidence relative to 0°, the frequency shift is Δf ≈ 6.9% (f_1), 1.6% (f2), 6.8% (f3), and 0.6% (f4) for TE polarization, and Δf ≈ 6.9% (f_1), 1.6% (f_2), 7.7% (f_3), and 1.1% (f_4) for TM polarization, with the largest shift (≈7.7%) occurring for the TM-mode third resonance. In terms of absorption magnitude, all four bands remain at or above 80% for both TE and TM modes up to 60° incidence, with the single exception of the TM-mode fourth resonance, which falls marginally to 79.6% at 60°; beyond 60° (at 75°), the absorption drops substantially for several bands (to as low as ≈50%). These results indicate that the proposed absorber maintains acceptable angular stability up to 60° incidence, whereas the response degrades considerably at larger oblique angles.

Table 3. Performance results of the proposed absorber under different polarization angles for TE and TM polarizations

Polarization angles	Mode	f_1 Resonance (GHz) Absorption (%)	f_2 Resonance (GHz) Absorption (%)	f_3 Resonance (GHz) Absorption (%)	f_4 Resonance (GHz) Absorption (%)
0°	TE	2.9 GHz- %99.4	6.3 GHz- %97.9	11.7 GHz- %98.2	17.6 GHz- %95.1
30°	TE	3 GHz- %99.2	6.3 GHz- %97.85	11.4 GHz- %98.18	17.7 GHz- %95.13
60°	TE	3.1 GHz- %99	6.4 GHz- %97.8	10.8 GHz- %98.1	17.8 GHz- %95.12
90°	TE	3.2 GHz- %99.3	6.4 GHz- %97.8	12.2 GHz- %98.1	17.8 GHz- %95
0°	TM	2.9 GHz- %99.4	6.3 GHz- %97.9	11.7 GHz- %98.2	17.6 GHz- %95.1
30°	TM	3 GHz- %99.44	6.3 GHz- %97.89	11.4 GHz- %98.2	17.7 GHz- %95.1
60°	TM	3.1 GHz- %99.4	6.4 GHz- %97.88	10.8 GHz- %98.18	17.8 GHz- %95.1
90°	TM	3.2 GHz- %99.4	6.4 GHz- %97.7	12.2 GHz- %98.2	17.8 GHz- %95

To quantify the polarization-insensitivity claim beyond the visual overlap of the curves in Figure 4, the data in Table 3 were further analyzed for φ = 0°, 30°, 60°, and 90°. The absorption magnitude at each resonance varies by no more than ≈0.4 percentage points across all polarization angles for both TE and TM modes (e.g., f_1: 99.0–99.4% (TE), 99.4–99.44% (TM); f_4: 95.0–95.13% (TE), 95.0–95.1% (TM)), with the minimum absorption across all polarization angles and bands remaining above 95%. The corresponding frequency shift, evaluated as $\Delta f(\%) = |f_\varphi - f_0|/f_0 \times 100$ between φ = 90° and φ = 0°, is Δf ≈ 10.3% (f_1), 1.6% (f_2), 4.3% (f_3), and 1.1% (f_4) for both TE and TM modes. These results confirm that, while the lowest-frequency resonance (f_1) exhibits a moderate shift in its center frequency with polarization angle, the absorption magnitude itself remains essentially unchanged (within ≈0.4 percentage points), substantiating the polarization-insensitive behavior of the proposed absorber in terms of absorption performance.

Figures 5, 6, and 7 present the E-field, H-field, and surface-current distributions of the proposed MSA at the resonance frequencies of 2.9 GHz, 6.3 GHz, 11.7 GHz, and 17.5 GHz. As can be observed from the field distributions, the electromagnetic energy is concentrated in specific regions of the structure. The localization of the electric and magnetic fields on the resonator indicates the excitation of strong resonances at the corresponding frequencies. These field concentrations indicate that the incident electromagnetic energy is effectively confined within the structure; the associated dielectric- and conductor-loss mechanisms responsible for the resulting high absorption performance are examined in detail below. Furthermore, the distinct field distributions observed at different resonance frequencies are linked to different resonant current paths, as detailed below, and support the multiband operating characteristic of the proposed MSA.

As shown in Figure 5, at 2.9 GHz and 11.7 GHz the electric field is predominantly concentrated along the arms of the outer square frame, whereas Figure 6 shows that the corresponding magnetic field is also strongly localized in the same regions. This indicates that these resonances primarily originate from the longer current path provided by the outer square resonator, representing the lower- and mid-frequency resonance modes. In contrast, Figure 5 demonstrates that at 6.3 GHz and 17.5 GHz the electric field is strongly confined around the inner cross-shaped resonator, while Figure 6 reveals a similar localization of the magnetic field in the same region. This observation indicates that the shorter current path associated with the cross element dominates the higher-frequency resonance modes. Furthermore, the strong magnetic-field localization observed in Figure 6 along the outer square frame at 2.9 and 11.7 GHz and along the cross arms at 6.3 and 17.5 GHz is consistent with the formation of anti-parallel current loops between the patterned metallic layer and the continuous ground plane. This is directly confirmed by the surface-current distributions shown in Figure 7, which compare the current vectors on the top resonator and on the ground plane at each of the four resonance frequencies and reveal that the two layers carry currents of opposite orientation, closing a current loop through the FR-4 layer. This behavior is a well-established signature of magnetic resonance in metal-backed metasurface absorbers. The resulting current distribution effectively confines the incident electromagnetic energy within the thin FR-4 dielectric layer sandwiched between the two metallic layers, thereby enhancing both dielectric and ohmic losses. Because the FR-4 layer (loss tangent = 0.025) is markedly lossier than copper (conductivity = 5.8×10^7 S/m), dielectric loss in the FR-4 substrate is expected to be the dominant absorption mechanism at all four resonances, with ohmic (conductor) loss in the patterned resonator and ground plane providing a comparatively smaller, though non-negligible, contribution, particularly at the higher-frequency (X- and Ku-band) resonances where surface currents and associated conductor losses increase. A quantitative separation of these two loss contributions via power-loss density integration over the dielectric and metallic domains lies beyond the scope of the S-parameter-based analysis presented here. A dedicated power-loss-density analysis that quantitatively separates these dielectric and ohmic contributions is therefore identified as a promising direction for future work. Consequently, improved impedance matching is achieved at the resonance frequencies, leading to the high absorption performance reported in this work.

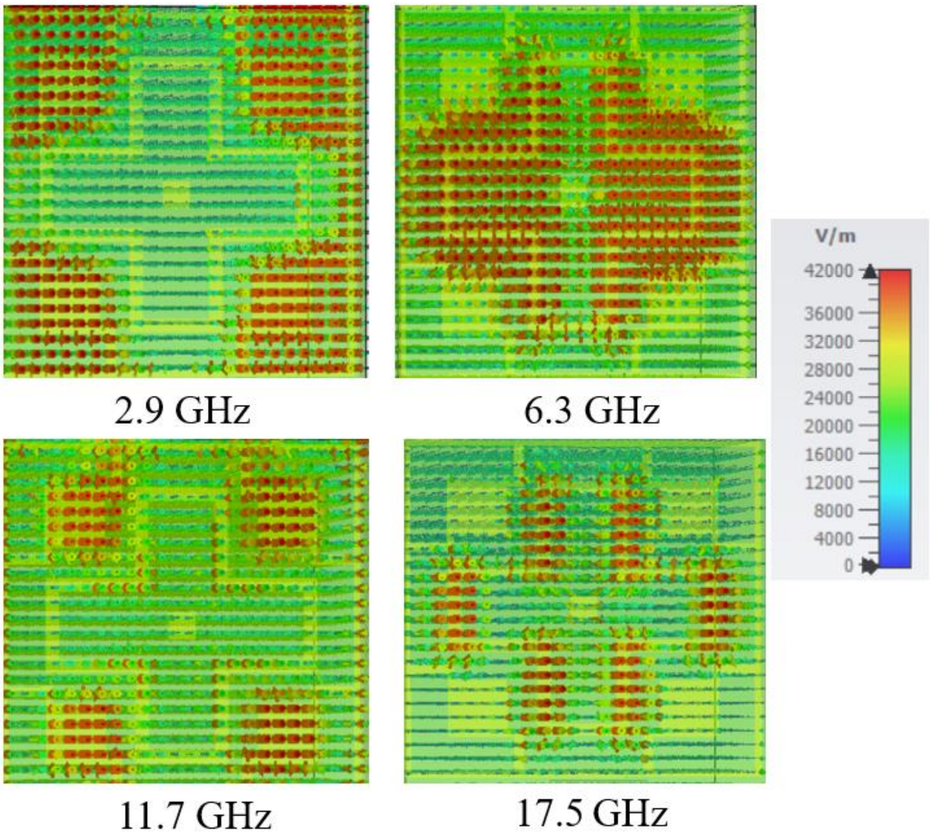

Figure 5. Electric field distribution of the proposed metasurface absorber

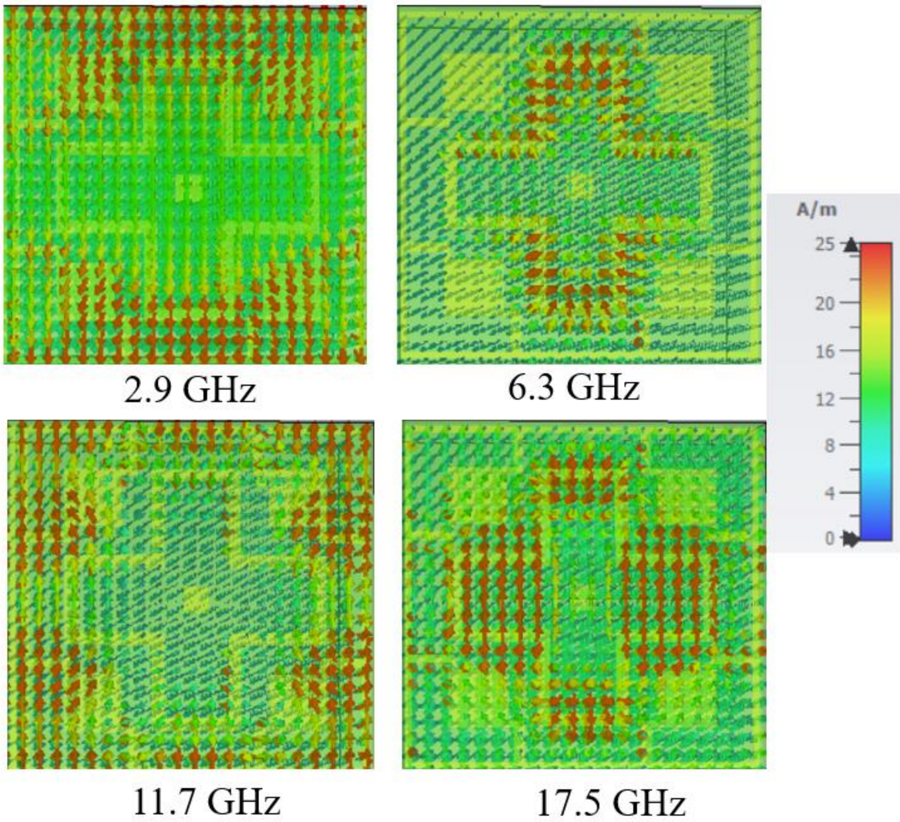

Figure 6. Magnetic field distribution of the proposed metasurface absorber

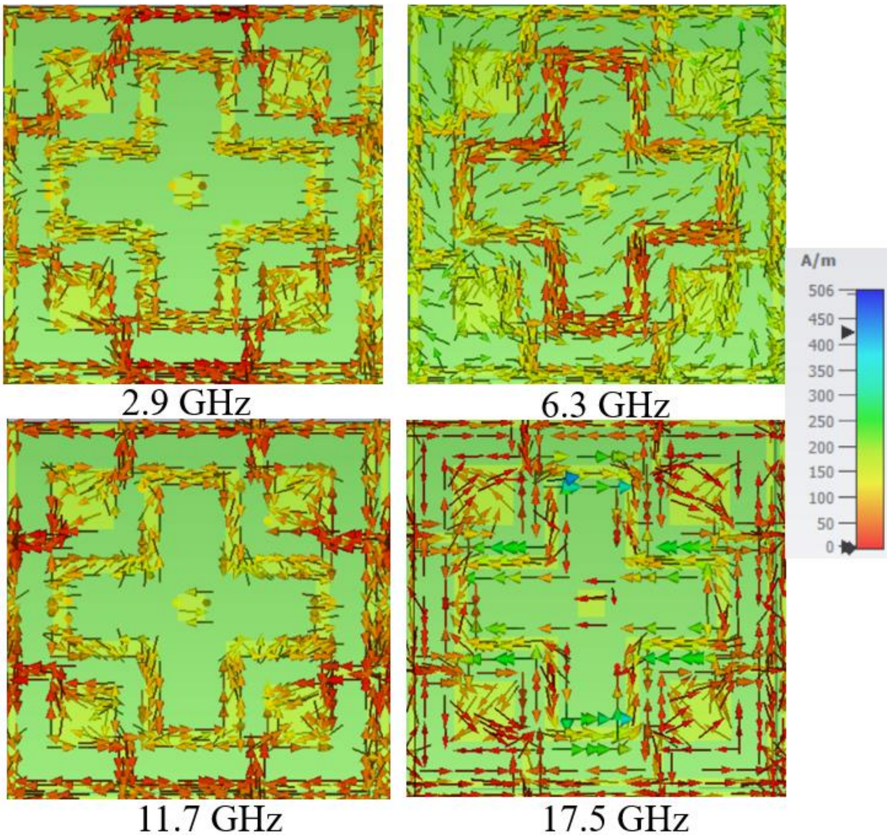

Figure 7. Surface current distribution of the proposed metasurface absorber

To explain the electromagnetic absorption mechanism of the proposed structure, the normalized impedance, ε_{eff}, μ_{eff}, and refractive index (n) are examined in Figure 8(a–d). In Figure 8(a), the real part of the normalized impedance Re(Z) approaches approximately 1 at the resonant frequencies of 2.9 GHz, 6.3 GHz, 11.7 GHz, and 17.5 GHz, while the imaginary part Im(Z) tends toward zero. This indicates good impedance matching with free space at these frequencies, leading to strong absorption. In Figure 8(b) and 8(c), the pronounced increase in the imaginary parts of ε and μ around the resonant frequencies is consistent with the simultaneous excitation of electric and magnetic resonances, as further supported by the surface-current distributions in Figure 7, which show anti-parallel current loops between the patterned resonator and the ground plane. In Figure 8(d), the increase in the imaginary part of the refractive index is likewise consistent with strong electromagnetic energy dissipation within these bands, subject to the retrieval-validity caveats discussed below. The justification, branch-selection criterion, and physical interpretation of this retrieval procedure for the present metal-backed, single-layer metasurface are discussed in detail immediately following Equation (4).

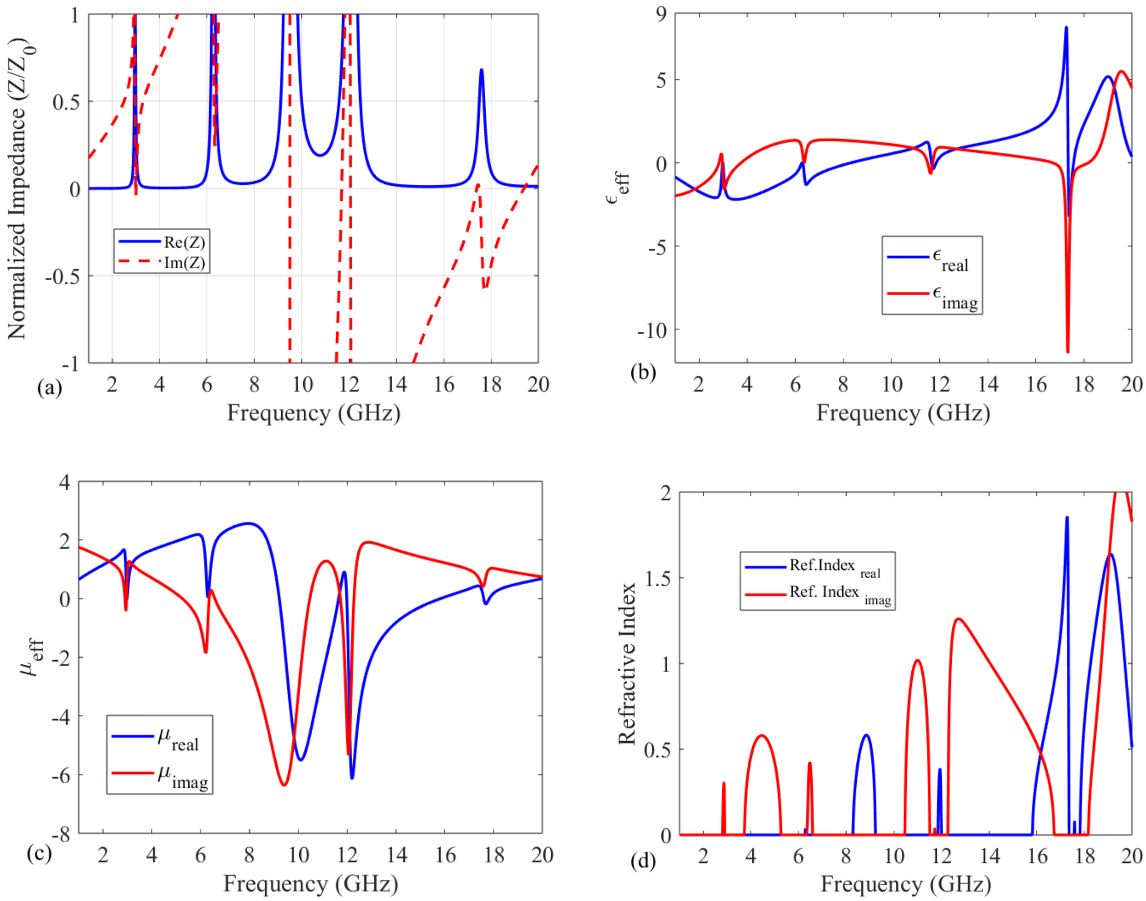

Figure 8. Frequency-dependent variations of (a) normalized impedance, (b) effective permittivity (ε), (c) effective permeability (μ), and (d) refractive index (n) of the proposed MSA

Figure 9(a–e) shows the effects of the geometrical parameters p, k, s, c, and h, respectively, on the S_{11} response of the proposed MSA. Variations in these parameters cause shifts in the resonance frequencies and changes in the reflection levels. The optimum values are determined as p=11 mm, k=1.3 mm, s=3.08 mm, c=3.6 mm, and h=1 mm, providing the desired multiband absorption performance.

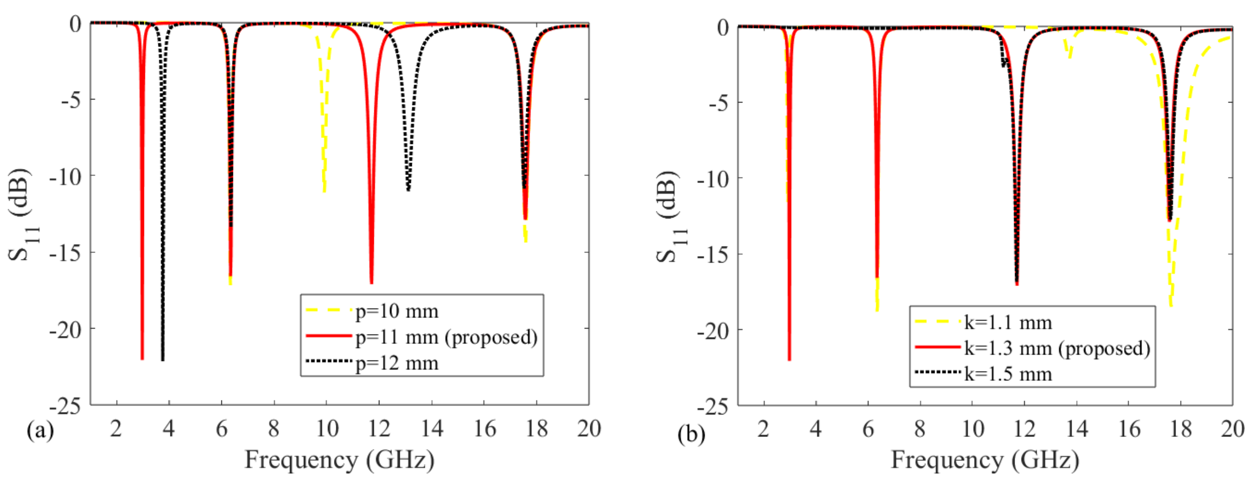

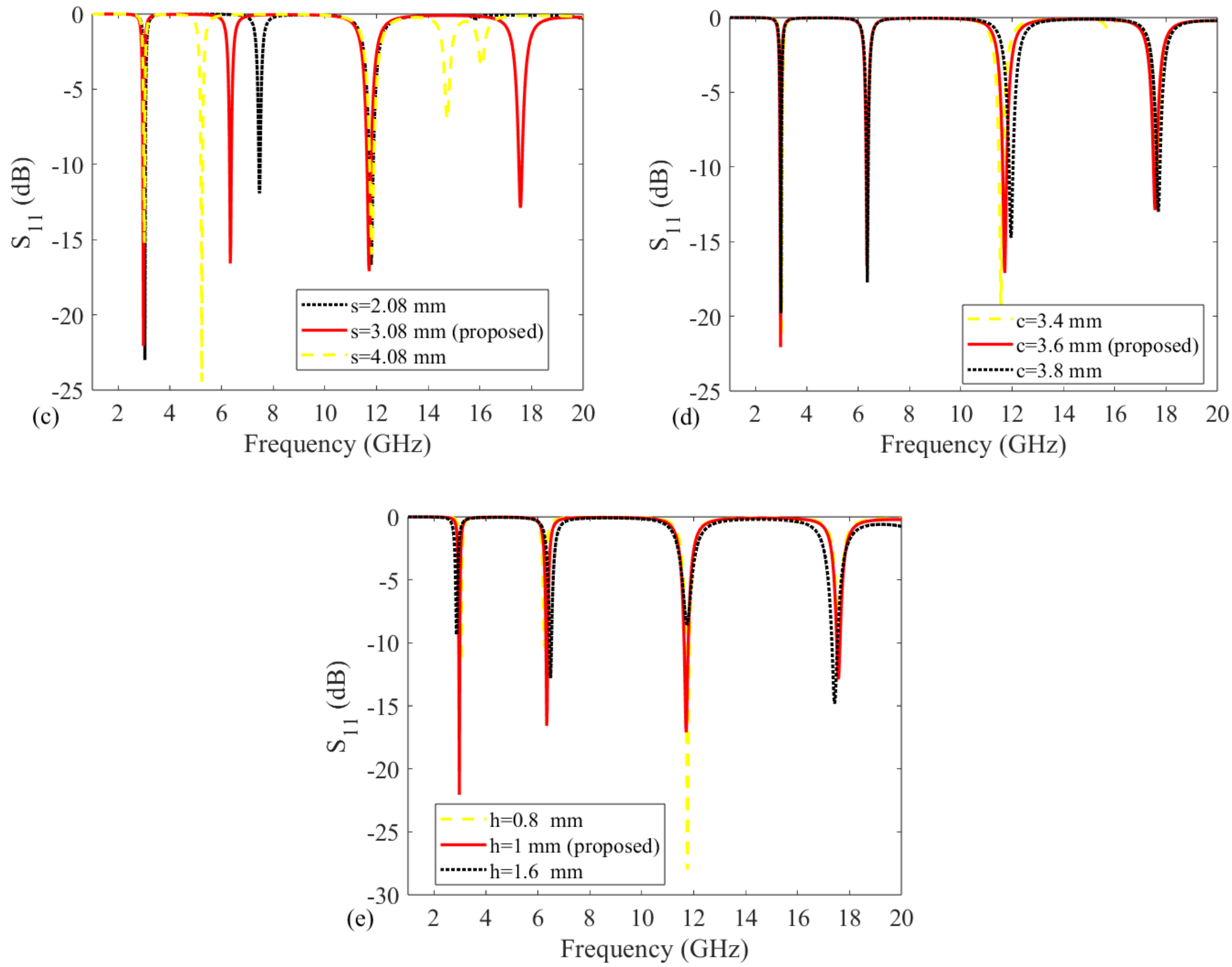

Figure 9. Effect of the geometrical parameters of the proposed MSA on the S_{11} absorption spectrum: (a) p, (b) k, (c) s, (d) c, and (e) h parameters

Figure 10 shows the RLC-based equivalent circuit model (ECM) developed in ADS to analyze the resonance mechanism of the proposed MSA at the circuit level and to independently validate the CST results. Figure 11 compares the S_{11} results obtained using ADS and CST. The presence of the four main resonances at similar frequencies in both approaches confirms that the ECM successfully represents the resonance behavior of the proposed structure.

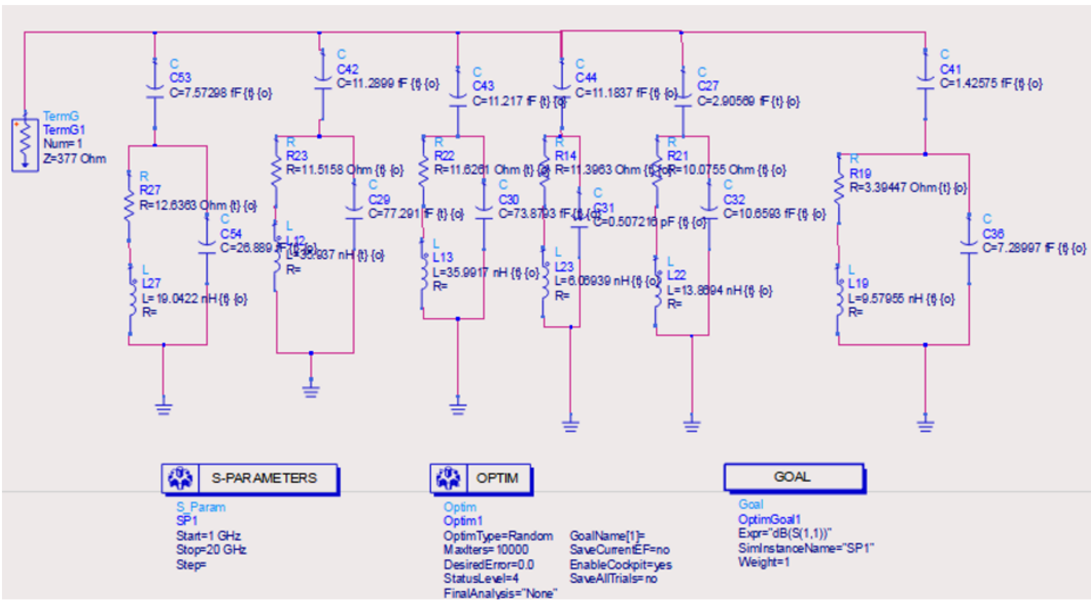

Figure 10. Equivalent circuit model (ECM) of the proposed metasurface absorber implemented in ADS

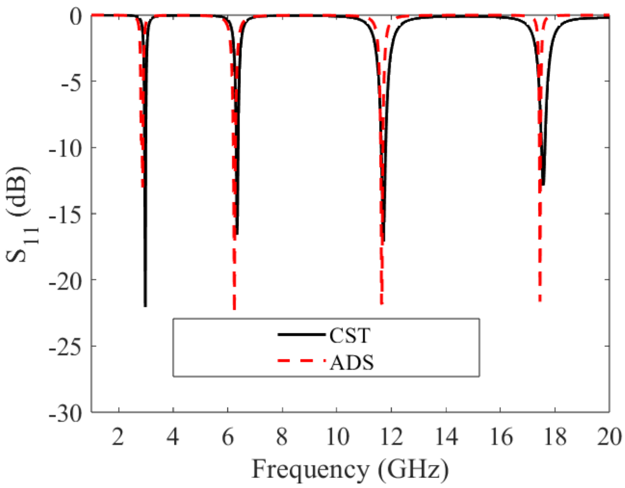

Figure 11. Comparison of the S_{11} simulation results obtained using ADS and CST for the proposed MSA

Table 4. Comparison of the proposed MSA with existing literature-based similar absorber structures

Ref.	Resonance Frequency	Absorp. Rate	Operating Frequency	Number of Bands	Material	Thickness	Incident Angle	Pol. Stab.	Meas. Stat.	BW	Finite-array
[25]	3.64 GHz, 5.99 GHz, 7.47 GHz and 10.01 GHz	>90	S, C, and X	4	FR-4	1.6 mm $\lambda=0.019\lambda_0$	Not reported	Not reported	Simulation only	0.15	Not performed
[26]	2.46 GHz, 6.25 GHz and 12.45 GHz	>99	S, C, and Ku	3	FR-4	1.6 mm $\lambda=0.013\lambda_0$	Not reported	Not reported	Measured (fabricated)	Not reported	Not performed
[27]	3.06 GHz, 3.9 GHz, and 5.97 GHz	>99	S and C	3	FR-4	2.2 mm $\lambda=0.022\lambda_0$	45	İns. (0°-90°)	Measured (fabricated)	Not reported	Performed
[28]	4.87 GHz, 7.49 GHz, 11.78 GHz, and 13.09 GHz	>99	C, X, and Ku	4	Rogers RT5870	1.575 mm $\lambda=0.025\lambda_0$	50	İns. (0°-20°)	Simulation only	0.2	Not performed
[29]	4.37 GHz, 7.08 GHz, 9.38 GHz, and 10.65 GHz	>99	C, and X	4	Rogers RT 5870	1.575 $\lambda=0.023\lambda_0$	80	Insensitive (0°-30°)	Simulation only	0.2	Not performed
[30]	6.41 GHz, 11.69 GHz, 15.55 GHz, and 17.82 GHz	>99	X, and Ku	4	FR-4	1.6 mm $\lambda=0.034\lambda_0$	45	Sensitive	Measured (fabricated)	Not reported	Performed
This work	2.9 GHz, 6.3 GHz, 11.7 GHz, and 17.5 GHz	>95	S, C, X, and Ku	4	FR-4	1 mm $\lambda=0.009\lambda_0$	60	İns. (0°-90°)	Simulation only	0.0064-0.0114	Not performed

Table 4 presents a comparative evaluation of the proposed metasurface absorber with similar studies reported in the literature in terms of resonant frequency, maximum absorption, operating frequency band, number of absorption bands, substrate material, substrate thickness, incident angle, polarization stability, experimental validation, bandwidth, and finite array analysis. Regarding the number of absorption bands, Refs. [26] and [27] report triple-band absorbers, whereas Refs. [25], [28], [29], [30], and the proposed design are all quad-band absorbers. In terms of operating frequency bands, the proposed absorber covers the S-, C-, X-, and Ku-bands within a single structure, while Ref. [25] covers the S-, C-, and X-bands, Ref. [28] covers the C-, X-, and Ku-bands, Ref. [29] covers only the C- and X-bands, and Ref. [30] covers the X- and Ku-bands. Among the triple-band designs, Ref. [26] operates in the S-, C-, and Ku-bands, whereas Ref. [27] is limited to the S- and C-bands. In terms of absorption performance, most of the studies in Refs. [26]–[30] achieve peak absorption levels of approximately 99%, while Ref. [25] reports about 90% absorption. The proposed absorber achieves absorption levels exceeding 95% at all resonant frequencies. Regarding the substrate material, FR-4 is employed in Refs. [25], [26], [27], and [30], whereas Rogers RT5870 is used in Refs. [28] and [29]. Similar to several previous studies, the proposed design also utilizes the low-cost and widely available FR-4 substrate. Regarding structural complexity, the proposed absorber and all compared designs in Table 4 (Refs. [25]–[30]) employ a single patterned metallic layer on a single dielectric substrate rather than a multilayer stack, so fabrication complexity across these designs is comparable and is governed mainly by minimum feature size and alignment tolerance rather than by layer count. In terms of substrate cost, the proposed design, together with Refs. [25], [26], [27], and [30], is implemented on low-cost FR-4, whereas Refs. [28] and [29] employ the substantially more expensive Rogers RT5870 laminate; the proposed FR-4-based design is therefore among the most cost-effective options in the comparison. In terms of substrate thickness, the proposed absorber has a thickness of 1 mm ($0.009\lambda_0$), which is the thinnest among the compared studies. The reported substrate thicknesses in the literature are 1.6 mm ($0.019\lambda_0$) in Ref. [25], 1.6 mm ($0.013\lambda_0$) in Ref. [26], 2.2 mm ($0.022\lambda_0$) in Ref. [27], 1.575 mm ($0.025\lambda_0$) in Ref. [28], 1.575 mm ($0.023\lambda_0$) in Ref. [29], and 1.6 mm ($0.034\lambda_0$) in Ref. [30]. With respect to angular stability, Refs. [25] and [26] do not report incident-angle performance, whereas maximum incident angles of 45°, 50°, 80°, and 45° are reported in Refs. [27], [28], [29], and [30], respectively. The proposed absorber maintains high absorption performance up to an incident angle of 60°. In terms of polarization stability, Refs. [27] and the proposed design exhibit polarization-insensitive performance over a polarization angle range of 0°–90°, while Refs. [28] and [29] demonstrate polarization insensitivity only over more limited ranges. In contrast, Ref. [30] reports a polarization-sensitive structure. Regarding experimental validation, physical prototypes were fabricated and measured in Refs. [26], [27], and [30], whereas Refs. [25], [28], [29], and the proposed work are based solely on numerical simulations. In terms of fractional bandwidth, values of 0.15 and 0.20 are reported in Refs. [25] and [28]–[29], respectively, while this metric is not provided in Refs. [26], [27], and [30]. The proposed design exhibits fractional bandwidths ranging from 0.0064 to 0.0114 (0.64%–1.14%, Table 1) across the four resonances, narrower than the values reported in Refs. [25] (0.15) and [28]–[29] (0.2). Furthermore, finite array analysis is reported only in Refs. [27] and [30], whereas neither the proposed work nor the remaining studies include this analysis. While each of Refs. [25]–[30] satisfies only a subset of these criteria, the proposed design simultaneously achieves four-band S/C/X/Ku coverage, a sub-0.01λ_0 thickness, absorption exceeding 95%, angular stability up to 60°, and full 0°–90° polarization insensitivity within a single structure.

4. Conclusions

In this study, a multiband MSA was numerically designed and simulated, demonstrating high performance in the S, C, X, and Ku bands. The proposed structure exhibits simulated peak absorption levels above 95% at 2.9, 6.3, 11.7, and 17.5 GHz, although the corresponding absorption bandwidths are narrow (fractional bandwidths of 0.64–1.14%, Table 1), which should be taken into account when assessing practical usefulness. In addition, the quantitative results in Tables 2 and 3 indicate polarization-insensitive behavior (absorption variation within approximately 0.4 percentage points across polarization angles) and acceptable angular stability, with absorption remaining generally at or above 80% for both TE and TM modes up to 60° incidence — with a single marginal exception (79.6%) for the TM-mode fourth resonance — while degrading substantially beyond 60°. The obtained numerical results indicate that the proposed design is a promising candidate for multi-band microwave absorption in applications such as RCS reduction and EMI/EMC mitigation. However, application-specific validation — including finite-array simulation, shielding-effectiveness analysis, and experimental measurement — is required before its practical applicability in these areas can be confirmed.

Nomenclature

RCS : Radar Cross Section
MSA : Metasurface Absorber
S_{11} : Reflection Coefficient
S_{21} : Transmission Coefficient
R : Power Reflection Coefficient (Reflectance), R = |S11|^2
T : Power Transmission Coefficient (Transmittance), T = |S21|^2
A : Absorption
ε_{eff} : Effective Permittivity
μ_{eff} : Effective Permeability
Z : Normalized Wave Impedance
n : Effective Refractive Index
k0 : Free-Space Wave Number
d : Structure Thickness (used in retrieval Equations (2)–(3))
h : Dielectric Substrate Thickness

Declaration of Conflict of Interests

The author declares that there is no conflict of interest. They have no known competing financial interests or personal relationships that could have appeared to influence the work reported in this paper.

References

[1.] Garg, P., Jain, P., A review of metamaterial absorbers and their application in sensors and radar cross-section reduction. Microwave and Optical Technology Letters 65 (2023) 387–411.

[2.] Mishra, N., Kumari, K., Chaudhary, R.K., An ultra-thin polarization independent quad-band microwave absorber-based on compact metamaterial structures for EMI/EMC applications. International Journal of Microwave and Wireless Technologies 10 (2018) 422–429.

[3.] Veselago, V.G., Electrodynamics of substances with simultaneously negative electrical and magnetic permeabilities. Soviet Physics Uspekhi 10 (1968) 509–514.

[4.] Pendry, J.B., Holden, A.J., Robbins, D.J., Stewart, W.J., Magnetism from conductors and enhanced nonlinear phenomena. IEEE Transactions on Microwave Theory and Techniques 47 (1999) 2075–2084.

[5.] Pendry, J.B., Schurig, D., Smith, D.R., Controlling electromagnetic fields. Science 312 (2006) 1780–1782.

[6.] Shelby, R.A., Smith, D.R., Schultz, S., Experimental verification of a negative index of refraction. Science 292 (2001) 77–79.

[7.] Wang, Y., Kong, Y., Xu, S., Li, J., Liu, G., Simulated studies of polarization-selectivity multi-band perfect absorber based on elliptical metamaterial with filtering and sensing effect. Photonics 10 (2023) 295.

[8.] Ozturk, G., Hasar, U.C., Ertugrul, M., Tutar, F., Corapsiz, M.F., Kurt, M., et al., An efficient cost effective wide-angle metasurface-based linear and circular polarization converter for X-, Ku- and K-band applications. Optics and Laser Technology 163 (2023) 109404.

[9.] Kurt, M., Ozturk, G., Ertugrul, M., Hepta-Band Ultra-Thin Metasurface Absorber for S-, C-, X-, Ku-, and K-Band Applications. Arabian Journal for Science and Engineering 50 (2025) 17813–17826.

[10.] Gong, Y., Morawski, R., Le-Ngoc, T., Metamaterial absorber structure for Tx-Rx antenna isolation improvement in full-duplex massive MIMO. IEEE Access 12 (2024) 64571–64588.

[11.] Ma, S., et al., Highly sensitive terahertz sensor based on graphene metamaterial absorber. Optics Communications 528 (2023) 129021.

[12.] Xiong, W., et al., Machine learning-driven design of optical transparency metamaterial absorbers with infrared-microwave compatible camouflage based on indium tin oxide. Science China Technological Sciences 68 (2025) 2020203.

[13.] Shi, Y., Cao, X., Li, S., Li, L., Invisible cloak design and application of metasurfaces on microwave absorption and RCS reduction. Electromagnetic Metamaterials and Metasurfaces: From Theory to Applications (2024) 287–350.

[14.] Singh, H., Gupta, A., Kaler, R.S., Singh, S., Gill, A.S., Designing and analysis of ultrathin metamaterial absorber for W-band biomedical sensing application. IEEE Sensors Journal 22 (2022) 10524–10531.

[15.] Ali, H.O., Al-Hindawi, A.M., Abdulkarim, Y.I., Karaaslan, M., New compact six-band metamaterial absorber based on Closed Circular Ring Resonator (CCRR) for radar applications. Optics Communications 503 (2022) 127457.

[16.] Kurt, M., Ozturk, G., Hasar, U.C., Ertugrul, M., Ultra-thin, polarization-insensitive, deca-band metasurface absorber based on a plus-shaped resonator with concentric circular arc elements. Optics and Laser Technology 199 (2026) 115001.

[17.] Babu, K.V., Sree, G.N.J., Design and circuit analysis approach of graphene-based compact metamaterial absorber for terahertz range applications. Optical and Quantum Electronics 55 (2023) 769.

[18.] Ren, Y., Cui, W., Li, Z., Zhang, L., Yang, Z., Lu, S., et al., Tunable broadband absorbers with ultra-high thermal emissivity for the MXene/Ti-based metamaterial. Renewable Energy 231 (2024) 120877.

[19.] Errajraji, K., Jebbor, N., Das, S., Islam, T., Madhav, B.T.P., El-Arrouch, T., Design and analysis of a multi-band miniaturized metamaterial absorber for wireless communication applications. Optical and Quantum Electronics 56 (2024) 232.

[20.] Soghi, S., Heidar, H., Haraty, M.R., Nayyeri, V., Single-layer broadband optically transparent metamaterial absorber using gold thin film. IEEE Transactions on Microwave Theory and Techniques 72 (2023) 3743–3752.

[21.] Ilchenko, M.Y., Zhivkov, O.P., Kamarali, R.V., Lutchak, O.V., Fedorchuk, O.P., V'yunov, O.I., et al., Modeling of electromagnetically induced transparency with RLC circuits and metamaterial cell. IEEE Transactions on Microwave Theory and Techniques 71 (2023) 5104–5110.

[22.] Yao, X., Huang, Y., Li, G., He, Q., Chen, H., Weng, X., et al., Design of an ultra-broadband microwave metamaterial absorber based on multilayer structures. International Journal of RF and Microwave Computer-Aided Engineering 32 (2022) e23222.

[23.] Hakim, M.L., et al., Polarization insensitivity characterization of dual-band perfect metamaterial absorber for K band sensing applications. Scientific Reports 11 (2021) 17829.

[24.] Öztürk, G., Hasar, U.C., Bute, M., Ertuğrul, M., Determination of constitutive parameters of strong-coupled bianisotropic metamaterials using oblique incidence scattering parameters. IEEE Transactions on Antennas and Propagation 69 (2020) 918–927.

[25.] Rabbani, M.G., Islam, M.T., Hoque, A., Bais, B., Albadran, S., Islam, M.S., Soliman, M.S., Orthogonal centre ring field optimization triple-band metamaterial absorber with sensing application. Engineering Science and Technology, an International Journal 49 (2024) 101588.

[26.] Chowdhury, M.Z.B., Islam, M.T., Ouda, M., Soliman, M.S., Alamri, S., Samsuzzaman, M., Design of an omega phi-shaped tri band metamaterial absorber with sensing application. Engineering Science and Technology, an International Journal 56 (2024) 101777.

[27.] Agrahari, R., Singh, S., Samantaray, D., Kumar, B., Bhattacharyya, S., Mahto, M., Jain, P.K., Triple-band metasurface absorber for RF energy harvesting applications. Microwave and Optical Technology Letters 65 (2023) 2252–2261.

[28.] Jahan, M.I., Faruque, M.R.I., Hossain, M.B., Khandaker, M.U., Elsayed, F., Salman, M., Osman, H., Quad-band metamaterial perfect absorber with high shielding effectiveness using double X-shaped ring resonator. Materials 16 (2023) 4405.

[29.] Jahan, M.I., Faruque, M.R.I., Hossain, M.B., An X-shaped triple split ring resonator-based metamaterial perfect absorber with quad-band incident and polarization angle insensitivity for C, X, and Ku band applications. Journal of Magnetism and Magnetic Materials 580 (2023) 170940.

[30.] Xia, Q., Zhang, J., Wang, Y., Li, T., Liu, B., Song, W., et al., A quad-band metamaterial microwave absorber based on elliptical and square ring resonators. AIP Advances 16 (2026).

How to Cite This Article

Kurt, M., Design of a Thin-Profile FR-4 Based Multi-Band Metasurface Absorber in S, C, X, and Ku Bands, 1(2027), 41158.
https://doi.org/10.36937/ben.2027.41158